INTERNATIONAL JOURNAL OF
NUMERICAL ANALYSIS AND MODELING
Volume 23, Number 3, Pages 374–389

doi: 10.4208/ijnam2026-1015

AN EFFICIENT RVE-EMC APPROACH FOR MULTISCALE EQUATIONS OF RANDOM HETEROGENEOUS MATERIALS

YANFU CHEN, XIXIN WU, ZIHAO YANG, JIEQIONG ZHANG, AND JUNFENG ZHAO*

Abstract. Resolving multiscale equations in heterogeneous materials presents significant computational challenges arising from rapid spatial oscillations and random variations in solutions induced by intricate microstructural configurations. This study proposes and analyzes a two-stage stochastic homogenization framework designed to efficiently compute homogenized solutions for multiscale diffusion equations. The methodology unfolds through two distinct phases. In the first stage, each realization of the random microstructure undergoes spatial homogenization through a representative volume element (RVE)-based approach, effectively replacing the original multiscale diffusion equation with a random counterpart featuring piecewise constant coefficients. Through ensemble-based Monte Carlo (EMC) averaging of diffusion coefficients, we reformulate the random diffusion equation into a deterministic diffusion problem with a random source term in the second stage. This critical reformulation enables the implementation of an efficient fixed-point iteration scheme for solving the resultant constant-coefficient diffusion equation. In addition, the convergence of the homogenized solution to the solution of multiscale diffusion equation is proved. Numerical examples are provided to demonstrate the ability and accuracy of the proposed method.

Key words. Stochastic homogenization, representative volume element, ensemble-based Monte Carlo, convergence, random heterogeneous materials.

1. Introduction

As is well known, heterogeneous materials are widely used in the field of engineering due to their excellent properties. Heterogeneous materials, such as concrete, short-fiber-reinforced composites, polymer composites and damaged composites [1, 2, 3], often have uncertainties originating from variations in microstructures or material parameters. Accurately evaluating the physical and mechanical responses of these materials requires quantifying the uncertainty of microstructure and material parameters. Mathematically, these responses can be described using multiscale partial differential equations (PDEs) with random, rapidly oscillating coefficients. A notable example is the class of random multiscale diffusion equations, which have been widely applied in the study of elastic mechanics, heat conduction, and electromagnetics of heterogeneous materials (see [4, 5, 6, 7, 8, 9]). Given the inherent randomness and highly fluctuating nature of material parameters, directly obtaining an accurate numerical solution to the multiscale diffusion problem in random heterogeneous materials is computationally demanding. The requirement for an extremely fine mesh and large-scale sampling leads to excessive computational costs in terms of both memory and processing time. Therefore, it is imperative to develop novel, efficient numerical methods to address these challenges.

Traditional stochastic homogenization theory [10, 11, 12] has been extensively developed to derive the homogenized diffusion equation from the original multiscale equation by formulating a random elliptic cell problem over the entire spatial domain. However, obtaining its numerical solution remains a significant challenge

Received by the editors on February 5, 2025 and accepted on June 17, 2025.
2000 *Mathematics Subject Classification.* 35B27, 60H15.
*Corresponding author.

due to computational complexity. To address this, various techniques, such as periodization and cut-off methods, have been introduced to locally approximate the homogenized coefficients [13, 14]. Nevertheless, ensuring the accuracy of these approximations necessitates a sufficiently large bounded domain, making numerical computations highly demanding.

Another widely used approach in engineering computations is the representative volume element (RVE) method, which is employed to estimate the effective parameters of highly heterogeneous or random composite materials. In this method, the cell problem is defined on a reasonably large representative cell [15, 16, 17, 18, 19, 20, 21], where the size of the cell does not necessarily tend to infinity. However, this method is commonly used in engineering and lacks a mathematical theoretical foundation. Once the homogenized coefficients are approximated, the primary computational challenge shifts to solving the random diffusion equation incorporating these coefficients. Directly applying Monte Carlo methods [22] or the stochastic Galerkin method [23, 24, 25, 26, 27] to solve this equation is computationally prohibitive. The Monte Carlo approach requires repeated evaluations of the random problem for different sample coefficients, leading to excessive computational cost. Similarly, the stochastic Galerkin method often results in a high-dimensional deterministic system, which demands substantial computational resources and may be infeasible for large-scale problems. To overcome the computational challenge, several approaches have been proposed in literature including variants of the ensemble method [28, 29, 30, 31] and the multi-modes method [32, 33, 34, 35]. Resolving multiscale equations in heterogeneous materials still exist significant computational challenges arising from rapid spatial oscillations and random variations in solutions induced by intricate microstructural configurations.

This paper proposes an effective strategy to address the computational challenges arising from the spatial fast oscillations and the inherent randomness of the solution to the multiscale diffusion equation of random heterogeneous materials. Building on the RVE method, the ensemble-based Monte Carlo (EMC) method and our previous work [35], we introduce a practical two-stage stochastic homogenization method to efficiently compute homogenized solutions for multiscale diffusion equations. The key advantage of the proposed method is its ability to decouple the computational difficulties caused by spatial fast oscillations and those resulting from randomness, enabling each to be addressed separately using distinct strategies. In the first stage, the RVE-based spatially homogenization technique is proposed to deal with the computational difficulty caused by the spatial fast oscillation of the solution. And the EMC method is applied to deal with the computational difficulty caused by the randomness of the solution in the second stage. Besides, we also prove the convergence of the homogenized solution to the solution of multiscale diffusion equation. It should be pointed out that we give a mathematical interpretation and justification for the RVE method.

The remainder of the paper is structured as follows. Section 2 describes the setting of the multiscale diffusion problem arising from the random heterogeneous materials. In Section 3, we introduce the RVE-EMC two-stage approach and related convergence analysis for the multiscale diffusion problem. Section 4 presents the finite element discretization and a detailed implementation algorithm for the proposed method. In Section 5, numerical experiments are conducted to demonstrate the effectiveness of the proposed method. Finally, Section 6 provides concluding remarks.

2. Problem setting

We consider the following multiscale diffusion equation with a randomly oscillating coefficient, which characterizes heterogeneous materials

$$-\operatorname{div}\left(A^{\varepsilon}(x,\omega)\nabla u^{\varepsilon}(x,\omega)\right) = f(x,\omega) \qquad \text{in } D\times\Omega, \tag{1a}$$

$$u^{\varepsilon}(x,\omega) = 0 \qquad \text{on } \partial D\times\Omega. \tag{1b}$$

Here $D\in\mathbb{R}^d$ represents a bounded spatial domain, and ω denotes a sample point belonging to the probability space $(\Omega,\mathcal{F},\mathbb{P})$. The expectation of a random variable $\mathbf{X}\in L^1(\Omega,\mathrm{d}\mathbb{P})$ is given by $\mathbb{E}(\mathbf{X}) := \int_\Omega \mathbf{X}(\omega)\mathrm{d}\mathbb{P}(\omega)$. The coefficient matrix $A^{\varepsilon}(x,\omega) = (a_{ij}^{\varepsilon}(x,\omega))_{1\le i,j\le d}$ exhibits rapid oscillations, while the right-hand-side term $f(x,\omega)$ represents a random field with a continuous and bounded covariance function. For the sake of simplicity, we assume $f(x,\omega)=f(x)$ throughout this paper, meaning that f is a deterministic function. The parameter ε represents the characteristic length scale of the microstructure in heterogeneous materials (Fig. 1), typically satisfying $0<\varepsilon\ll 1$. Let $Q := (0,1)^d$ be the unit cell, and define $Q+\mathbf{k} := (k_1,k_1+1)\times(k_2,k_2+1)\times\cdots\times(k_d,k_d+1)$ for $\mathbf{k}=(k_1,k_2,\cdots,k_d)^T$ with $k_i\in\mathbb{Z}$. Furthermore, let $D\subset\mathbb{R}^d$ be a bounded domain expressed as $D=\cup_{\mathbf{k}\in\mathbb{Z}^d} D_{\mathbf{k}}$, where $D_{\mathbf{k}} = D\cap\varepsilon(Q+\mathbf{k})$. For a positive integer $M\in\mathbb{Z}^+$, we define $\mathcal{Q}_M := MQ = (0,M)^d$ and $\mathcal{Q}_M^{\mathbf{k}} = MQ+M\mathbf{k}$.

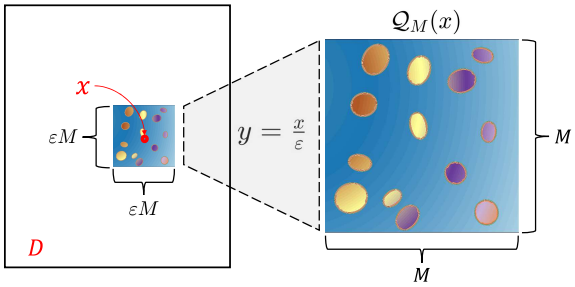

FIGURE 1. For a point x in computational domain $D\subset\mathbb{R}^2$, a square region centered at x is chosen as the RVE. The cell $\mathcal{Q}_M(x)$ is obtained via the mapping $y=\frac{x}{\varepsilon}$. The pseudo-color plot of $A(\frac{x}{\varepsilon},\omega)$ (right figure) illustrates the microstructure on cell $\mathcal{Q}_M(x)$.

Following prior studies [10, 11, 12], we assume that $A(\frac{x}{\varepsilon},\omega)\in\mathcal{M}(\alpha,\beta;D)$ is stationary, satisfying

$$A\Big(\frac{x}{\varepsilon}+\mathbf{k},\omega\Big) = A\Big(\frac{x}{\varepsilon},\tau_{\mathbf{k}}\omega\Big) \qquad \text{for any } \mathbf{k}\in\mathbb{Z}^d, \text{ a.e. in } D \text{ and } \mathbb{P}\text{-a.s.}, \tag{2}$$

Here $\tau_{\mathbf{k}}$ is an ergodic measure-preserving transformation, meaning that

$$\tau_{\mathbf{k}}E = E \quad \forall E\in\mathcal{F} \quad \text{implies that} \quad \mathbb{P}(E)=0 \text{ or } 1. \tag{3}$$

Additionally, we assume $A(\frac{x}{\varepsilon},\omega)\in\mathcal{M}(\alpha,\beta;D)$, where $\mathcal{M}(\alpha,\beta;D)$ denotes the set of invertible real-valued $d\times d$ matrices $A=A(\cdot,\omega)$ whose entries belong to $L^\infty(D)$ and satisfy $\mathbb{P}$-almost surely

$$\alpha|\xi|^2 \le (A\xi,\xi) \le \beta|\xi|^2 \qquad \text{for any } \xi\in\mathbb{R}^d \text{ and a.e. in } D. \tag{4}$$

Here $(\cdot,\cdot)$ represents the standard inner product in $\mathbb{R}^d$ and $|\xi|^2=(\xi,\xi)$.

3. RVE-EMC two-stage stochastic homogenization method

The objective of this section is to present the RVE-EMC two-stage stochastic homogenization method for solving problem (1) and to analyze its convergence. The methodology consists of two distinct phases, as illustrated in Fig. 2. In the first stage, the RVE-based homogenization method is employed to solve the oscillation problem, and the heterogeneous material characterized by the random coefficients $A(\frac{x}{\varepsilon},\omega)$ is approximated by the equivalent material with the random coefficients $\hat{A}(x,\omega)$, which is a constant matrix within each RVE for given ω. In the second stage, the EMC-based fixed-point iterative method is utilized to solve the random problem, and this process ultimately yields the homogenized material with the deterministic coefficient $\mathbb{E}(\hat{A}(x,\omega))$, representing the expected behavior of the effective material properties.

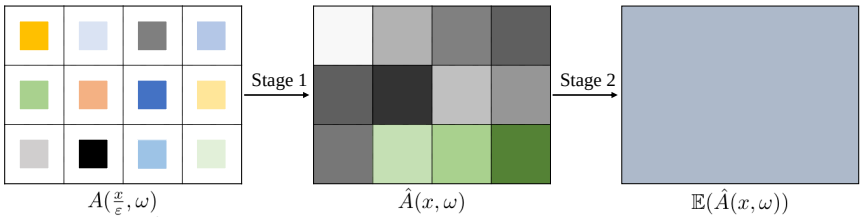

FIGURE 2. Framework of the two-stage stochastic homogenization method.

3.1. RVE-based homogenization method for oscillation problem. As illustrated in Fig. 1, for each given sample ω and any point $x \in D$, a $\mathcal{Q}_M(x)$ with $|\mathcal{Q}_M(x)| = M^d$ is derived from the RVE by using the mapping $y = \frac{x}{\varepsilon}$. The cell $\mathcal{Q}_M(x)$ preserves a structural similarity to the region surrounding x in domain D. Under this mapping, the coefficient $A^\varepsilon(x,\omega)$ can be rewritten as $A(y,\omega)$ within the cell $\mathcal{Q}_M(x)$. The differential operator with respect to x is then expressed as

$$\nabla_x \to \nabla_x + \frac{1}{\varepsilon}\nabla_y. \tag{5}$$

We define the following differential operators

$$\mathcal{L}_1(\omega) = -\nabla_y \cdot (A(y,\omega)\nabla_y)\,, \tag{6a}$$

$$\mathcal{L}_2(\omega) = -\nabla_y \cdot (A(y,\omega)\nabla_x) - \nabla_x \cdot (A(y,\omega)\nabla_y)\,, \tag{6b}$$

$$\mathcal{L}_3(\omega) = -\nabla_x \cdot (A(y,\omega)\nabla_x)\,. \tag{6c}$$

By performing an asymptotic expansion $u^\varepsilon(x,\omega)$ [7, 15], we obtain

$$u^\varepsilon(x,\omega) = u^0(x,y,\omega) + \varepsilon u^1(x,y,\omega) + +\varepsilon^2 u^2(x,y,\omega)\cdots\,, \tag{7}$$

where

$$u^1(x,y,\omega) = \mathbb{N}_{e_i}(x,y,\omega)e_i \cdot \nabla_x u^0(x,y,\omega). \tag{8}$$

Substituting (7) and (5) into (1), we derive the following expression

$$f(x) = \varepsilon^{-2}\mathcal{L}_1 u^0 + \varepsilon^{-1}(\mathcal{L}_1 u^1 + \mathcal{L}_2 u^0) + \varepsilon^0(\mathcal{L}_1 u^2 + \mathcal{L}_2 u^1 + \mathcal{L}_3 u^0) + \cdots\,. \tag{9}$$

Comparing the coefficients of ε^l (where $l = -2,-1,0,1,\ldots$), we obtain

$$\mathcal{L}_1 u^0 = 0, \tag{10a}$$

$$\mathcal{L}_1 u^1 + \mathcal{L}_2 u^0 = 0, \tag{10b}$$

$$\mathcal{L}_1 u^2 + \mathcal{L}_2 u^1 + \mathcal{L}_3 u^0 = f(x). \tag{10c}$$

Expanding (10a), we obtain

$$-\nabla_y \cdot \big(A(y,\omega)\nabla_y u^0(x,y,\omega)\big) = 0. \tag{11}$$

Thus, $u^0(x,y,\omega) = u^0(x,\omega)$ indicating that u^0 is independent of y.

Expanding (10b) and utilizing (8), we derive

$$\nabla_y \cdot \big(A(y,\omega)\nabla_y u^1(x,y,\omega)\big) + \nabla_y \cdot \big(A(y,\omega)\nabla_x u^0(x,\omega)\big) = 0. \tag{12}$$

The cell function $\mathbb{N}_{e_i}(y,\omega)$ is defined as the solution to the following cell problem on $\mathcal{Q}_M$

$$-\mathrm{div}\big[A(y,\omega)(e_i + \nabla \mathbb{N}_{e_i}(y,\omega))\big] = 0 \qquad \text{in } \mathcal{Q}_M, \tag{13a}$$

$$\mathbb{N}_{e_i}(y,\omega) \text{ is } \mathcal{Q}_M\text{-periodic.} \tag{13b}$$

It is important to note that x can be treated as a parameter in (13).

By integrating over the cell $\mathcal{Q}_M(x)$, the homogenized coefficient $\hat{A}(x,\omega)$ can be defined, with its (i,j)-th component given by

$$\hat{a}_{ij}(x,\omega) := \frac{1}{|\mathcal{Q}_M(x)|}\int_{\mathcal{Q}_M(x)} (e_i + \nabla \mathbb{N}_{e_i}(y,\omega))^T A(y,\omega)(e_j + \nabla \mathbb{N}_{e_j}(y,\omega))\mathrm{d}y. \tag{14}$$

The composite material with the oscillatory coefficient matrix $A^\varepsilon(x,\omega)$ is thus approximated by the equivalent matrix $\hat{A}(x,\omega)$. Here, M is a parameter that balances computational efficiency and accuracy. In numerical simulations, $M = \mathcal{O}(1)$ is typically chosen. The equivalent matrix $\hat{A}(x,\omega)$ remains constant within each block $\mathcal{Q}_M$ and serves as a coarse-grained approximation of the original matrix $A^\varepsilon(x,\omega)$. While the material is homogeneous within each block, heterogeneity is preserved across different blocks (see Fig. 2). Moreover, to approximate the solution of the original random diffusion equation (1), we solve the following homogenized system

$$-\mathrm{div}(\hat{A}(x,\omega)\nabla \hat{u}(x,\omega)) = f(x) \qquad \text{in } D, \tag{15a}$$

$$\hat{u}(x,\omega) = 0 \qquad \text{on } \partial D. \tag{15b}$$

However, the fluctuations in $\hat{A}(x,\omega)$ lead to high computational costs, particularly when ε is small and $M = \mathcal{O}(1)$. To address this challenge, we employ the EMC method [28, 29, 30, 31] in the second stage, providing an efficient means of solving (15).

3.2. EMC-based fixed-point iterative method for random problem. Let H be a Hilbert space, and let $V \in H$ be a Banach space. The dual space of V, denoted by V^*, consists of all bounded linear functionals on V. We consider the variational formulation of the homogenized equation (15), seeking $\hat{u}(x,\omega) \in V$ such that

$$\mathcal{D}(\hat{u}, v; \omega) = F(v) \quad \forall v \in V, \tag{16}$$

where $F(\cdot) \in V^*$ and $\mathcal{D}(\cdot,\cdot;\omega) : V \times V \to \mathbb{R}$ is an ω-dependent bilinear form defined by

$$\mathcal{D}(\hat{u}, v; \omega) = \big(\hat{A}(x,\omega)\nabla \hat{u}(x,\omega), \nabla v\big) \quad F(v) = \big(f, v\big). \tag{17}$$

According to the Proposition 2.1 in [30], problem (16) has a unique solution $u(x,\omega) \in V$ for each ω.

We decompose $\mathcal{D}(\hat{u}, v; \omega)$ as follows

$$\mathcal{D}(\hat{u}, v; \omega) = \mathcal{D}_0(\hat{u}, v) + \mathcal{D}_1(\hat{u}, v; \omega), \tag{18}$$

where

$$\mathcal{D}_0(\hat{u}, v) = \big(A^0(x)\nabla\hat{u}(x,\omega), \nabla v\big), \tag{19a}$$

$$\mathcal{D}_1(\hat{u}, v; \omega) = \big((\hat{A}(x,\omega) - A^0(x))\nabla\hat{u}(x,\omega), \nabla v\big). \tag{19b}$$

Here, $A^0(x) = (\mu^0_{ij,L}(x))$ is the ensemble mean of $\hat{A}(x,\omega)$, defined as

$$\mu^0_{ij,L}(x) = \frac{1}{L}\sum_{s=1}^{L} \hat{a}_{ij}(x,\omega_s). \tag{20}$$

Here, L denotes the number of Monte Carlo samples. Substituting (18) into (16), we obtain the variational form of the spatially homogenized diffusion equation (15)

$$\mathcal{D}_0(\hat{u}, v) = F(v) - \mathcal{D}_1(\hat{u}, v; \omega). \tag{21}$$

We now present the main iterative algorithm for solving (21) as follows

Step 1 Compute $U_0 \in V$ by solving

$$\mathcal{D}_0(U_0, v) = F(v) \quad \forall v \in V. \tag{22}$$

Step 2 For each $\omega \in \Omega$, determine $\{U_n = U_n(\omega)\}_{n\geq 1} \subset V$ recursively by solving

$$\mathcal{D}_0(U_n, v) = F(v) - \mathcal{D}_1(U_{n-1}, v; \omega) \quad \forall v \in V. \tag{23}$$

Repeat *Step 1* and *Step 2* for the Monte Carlo samples $\omega_s (s = 1, 2, \cdots, L)$, and the EMC approximation solution of (15) is given by

$$\hat{u}(x,\omega) = \frac{1}{L}\sum_{s=1}^{L} U_n(x,\omega_s). \tag{24}$$

The iterative equations (22) and (23) involve the same deterministic coefficients and a random source. Consequently, an LU direct solver can be employed to obtain numerical solutions efficiently, leading to significant computational cost savings.

3.3. Convergence of the method.

Lemma 3.1. *Suppose that $A(\frac{x}{\varepsilon}, \omega)$ satisfies the stationarity assumption given in (2). Then, the equivalent matrix $\hat{A}(x,\omega)$ can be expressed as*

$$\hat{A}(x,\omega) = \mathbb{E}(\hat{A}^0(\omega)) + \delta A_1(x,\omega), \tag{25}$$

where $\hat{A}^0(\omega)$ represents the equivalent matrix defined within each block $D \cap \varepsilon\mathcal{Q}^{\mathbf{k}}_M$, and $A_1(x,\omega) = (a^1_{ij}(x,\omega))$ with $a^1_{ij} \in L^2(\Omega, L^\infty(D))$. Additionally, the term δ is defined as $\delta := \max_{1\leq i,j\leq d}\sqrt{\mathbb{V}ar(\hat{a}^0_{ij}(\omega))}$. Furthermore, if the uniform mixing coefficient of $A(\frac{x}{\varepsilon}, \omega)$ satisfies the following growth condition

$$\gamma(s) \leq c(1+s)^{-\theta} \quad \text{for some } \theta > 0 \text{ and } \forall s > 0, \tag{26}$$

then there exists a constant $\zeta = \zeta(\theta, \alpha, d) > 0$ such that

$$\delta \leq CM^{-\zeta/2}. \tag{27}$$

Remark 3.2. *The proof of Lemma 3.1 follows directly from Theorem 3.1 and 4.2 in* [35].

Lemma 3.3. *Suppose that $A(\frac{x}{\varepsilon}, \omega) \in \mathcal{M}(\alpha, \beta; D)$ satisfies the stationarity assumption given in (2). If $\delta < 1$ and $f \in L^2(D)$, then the following error estimate holds*

$$\mathbb{E}\big(\|\hat{u}(x,\omega) - U_n(x,\omega)\|^2_{H^1(D)}\big) \leqslant C_1\delta^{2N}\|f\|^2_{L^2(D)}. \tag{28}$$

for some positive constant C_1 independent of δ.

Remark 3.4. *The proof of Lemma 3.3 follows from Theorem 3.2 in* [36] *and Remark 4 in* [30].

Theorem 3.5. *Let $M = C\varepsilon^{-\sigma}$ with $\sigma \in (0,1)$, and let u^ε be the solution of original multiscale problem (1). Assume that $f \in L^2(D)$ and that $A(\frac{x}{\varepsilon}, \omega) \in \mathcal{M}(\alpha, \beta; D)$ satisfies the stationarity assumption (2) and is $\mathcal{Q}_M$-periodic for $\mathbb{P}$-almost all $\omega \in \Omega$. Then, the following holds*

$$\lim_{\varepsilon \to 0} \mathbb{E}\left(\|u^\varepsilon(x,\omega) - U_n(x,\omega)\|^2_{L^2(D)} \right) = 0. \tag{29}$$

Proof. From Lemma 3.3, we obtain

$$\mathbb{E}\Big(\|\hat{u}(x,\omega) - U_n(x,\omega)\|^2_{L^2(D)} \Big) \leq C_1 \delta^{2N} \|f\|^2_{L^2(D)}. \tag{30}$$

Since $M = C\varepsilon^{-\sigma}$ with $\sigma \in (0,1)$, it follows from Lemma 3.1 that

$$\lim_{\varepsilon \to 0} \mathbb{E}\Big(\|\hat{u}(x,\omega) - U_n(x,\omega)\|^2_{L^2(D)} \Big) = 0. \tag{31}$$

By Theorem 6.1 in [37], for a given $\omega \in \Omega$, we have

$$\begin{aligned} u^\varepsilon(x,\omega) &\rightharpoonup \hat{u}(x,\omega) \quad \text{weakly in } H^1_0(D) \text{ as } \varepsilon \to 0, \\ u^\varepsilon(x,\omega) &\to \hat{u}(x,\omega) \quad \text{strongly in } L^2(D) \text{ as } \varepsilon \to 0. \end{aligned}$$

By the triangle inequality, we obtain

$$\begin{aligned} \lim_{\varepsilon \to 0} \mathbb{E}\left(\|u^\varepsilon(x,\omega) - U_n(x,\omega)\|^2_{L^2(D)} \right) &\leqslant \lim_{\varepsilon \to 0} \mathbb{E}\left(\|u^\varepsilon(x,\omega) - \hat{u}(x,\omega)\|^2_{L^2(D)} \right) \\ &\quad + \lim_{\varepsilon \to 0} \mathbb{E}\Big(\|\hat{u}(x,\omega) - U_n(x,\omega)\|^2_{L^2(D)} \Big) = 0. \end{aligned} \tag{32}$$

This completes the proof. □

4. Numerical implementation of the method

In this section, we address the implementation aspects of the proposed RVE-EMC two-stage stochastic homogenization method.

4.1. finite element discretization. Let $\{\omega_s\}_{s=1}^L$ be L independent and identically distributed (i.i.d.) random samples from the sample space Ω. Define $\mathbb{T}_h$ as a quasi-uniform partition of the cell $\mathcal{Q}_M$, such that $\overline{\mathcal{Q}_M} = \cup_{K_\mathbf{k} \in \mathbb{T}_h} \overline{K_\mathbf{k}}$. We assume that the partition $\mathbb{T}_h$ forms a body-fitted grid aligned with the coefficient matrix $A(y, \omega_s)$. Let $\mathbb{V}^h_r$ denote the standard finite element space of degree r, defined as

$$\mathbb{V}^h_r := \{v \in H^1_{per}(\mathcal{Q}_M); v|_{K_\mathbf{k}} \text{ is a polynomial of degree } r \text{ for each } K_\mathbf{k} \in \mathbb{T}_h\}. \tag{33}$$

Here, the periodic Sobolev space is given by

$$H^1_{per}(\mathcal{Q}_M) = \{v \in H^1(\mathcal{Q}_M); \text{ such that } v \text{ is } \mathcal{Q}_M\text{-periodic}\}.$$

The finite element cell solutions $\mathbb{N}^h_{e_i}(y, \omega_s)$ are defined as the solutions to

$$\big(A(y,\omega_s)(e_i + \nabla \mathbb{N}^h_{e_i}(y,\omega_s)), \nabla v^h\big)_{\mathcal{Q}_M} = 0 \qquad \forall v^h \in \mathbb{V}^h_r, \tag{34}$$

where $(u^h, v^h)_{\mathcal{Q}_M}$ denotes the standard L^2 inner product over $\mathcal{Q}_M$. Using the finite element cell solutions $\mathbb{N}^h_{e_i}(y, \omega_s)$, the (i,j)-th component of the approximate equivalent matrix equivalent matrix $\hat{A}^h(x, \omega_s)$ in block $D \cap \varepsilon\mathcal{Q}_M$ is given by

$$\hat{a}^h_{ij}(\omega_s) = \frac{1}{|\mathcal{Q}_M|} \int_{\mathcal{Q}_M} (e_i + \nabla \mathbb{N}^h_{e_i}(y,\omega_s))^T A(y,\omega_s)(e_j + \nabla \mathbb{N}^h_{e_j}(y,\omega_s)) \mathrm{d}y. \tag{35}$$

We define the empirical mean and variance for each component of $\hat{A}^h(\omega_s)$ in block $D \cap \varepsilon \mathcal{Q}_M$ as

$$\mu_{ij,L} := \mu_L\left(\hat{a}_{ij}^h(\omega_s)\right) = \frac{1}{L}\sum_{s=1}^{L} \hat{a}_{ij}^h(\omega_s), \tag{36a}$$

$$\sigma_{ij,L} := \sigma_L\left(\hat{a}_{ij}^h(\omega_s)\right) = \frac{1}{L-1}\sum_{s=1}^{L} \left(\hat{a}_{ij}^h(\omega_s) - \mu_{ij,L}\right)^2. \tag{36b}$$

By the strong law of large numbers [10], for sufficiently large L, we approximate $\mathbb{E}(\hat{a}_{ij}^h(\omega_s))$ using $\mu_{ij,L}$.

Let $\mathbb{T}_{h_0}$ be a quasi-uniform partition of computational domain D with mesh size h_0 such that $\overline{D} = \cup_{K\in\mathbb{T}_{h_0}} \overline{K}$. Define $\mathbb{V}_r^{h_0}$ as the standard finite element space of order r over $\mathbb{T}_{h_0}$

$$\mathbb{V}_r^{h_0} := \{v \in H_0^1(D); v|_K \text{ is a polynomial of degree } r \text{ for each } K \in \mathbb{T}_{h_0}\}. \tag{37}$$

The finite element approximation of the first mode function U_0 is given by

$$\left(\mu_L \nabla U_0^{h_0}(x), \nabla v^{h_0}\right)_D = (f, v^{h_0})_D \qquad \forall v^{h_0} \in \mathbb{V}_r^{h_0}. \tag{38}$$

Subsequently, we iteratively compute U_n using the following equation

$$\left(\mu_L \nabla U_n^{h_0}(x), \nabla v^{h_0}\right)_D = (f, v^{h_0})_D - \left(\mu_L \nabla U_{n-1}^{h_0}(x), \nabla v^{h_0}\right)_D \qquad \forall v^{h_0} \in \mathbb{V}_r^{h_0}. \tag{39}$$

Since direct simulations of the random diffusion equation (1) are computationally expensive, we use the empirical mean $\mathbb{E}(\hat{u}(x,\omega))$ of the equivalent solution to (15) as a reference to evaluate the efficiency and accuracy of the proposed method. Let $\mathbb{T}_{h_1}$ be a quasi-uniform partition of the computational domain D with mesh size h_1, such that $\overline{D} = \cup_{K\in\mathbb{T}_{h_1}} \overline{K}$. Define $\mathbb{V}_r^{h_1}$ as the standard finite element space of order r

$$\mathbb{V}_r^{h_1} := \{v \in H_0^1(D); v|_K \text{ is a polynomial of degree } r \text{ for each } K \in \mathbb{T}_{h_1}\}. \tag{40}$$

Let $\hat{u}^{h_1}(x,\omega_s)$ be the solution to (15) for $\omega = \omega_s$, given by

$$\left(\hat{A}^h(\omega_s)\nabla \hat{u}^{h_1}(x,\omega_s), \nabla v^{h_1}\right)_D = (f, v^{h_1})_D \qquad \forall v^{h_0} \in \mathbb{V}_r^{h_1}. \tag{41}$$

4.2. Algorithm procedure. The algorithmic procedure for the RVE-EMC two-stage stochastic homogenization method is outlined as follows

(1) Generate a set of independent and identically distributed (i.i.d.) samples $\{\omega_s\}_{s=1}^L$. For each sample ω_s, construct a body-fitted and quasi-uniform partition of the cell $\mathcal{Q}_M$ according to $A(y,\omega_s)$, where $y \in \mathcal{Q}_M$.
(2) Compute the finite element cell solutions $\mathbb{N}_{e_i}^h(y,\omega_s)$ by solving the problem in equation (34) and the (i,j)-th entry of the equivalent matrix $\hat{A}^{0,h}(\omega_s)$ using equation (35).
(3) Calculate the (i,j)-th component of the empirical mean matrix μ_L by using equation (36).
(4) Solve equations (38) and (39) to obtain the finite element approximation of the REV-EMC two-stage stochastic homogenization solution for the random diffusion equation in (1).

The algorithmic procedure for computing the reference solution is as follows

(1) Generate a set of i.i.d. samples $\{\omega\}_{s=1}^L$. For each sample ω_s, construct a body-fitted and quasi-uniform partition of the cell $\mathcal{Q}_M$ according to $A(y,\omega_s)$, where $y \in \mathcal{Q}_M$.

(2) Compute a set of finite element cell solutions $\mathbb{N}_{e_i}^h(y,\omega_s)$ by solving cell problem in equation (34) and the equivalent matrix $\hat{A}^h(\omega_s) = \left(\hat{a}_{ij}^h(\omega_s)\right)$ using equation (35).
(3) For each sample ω_s, solve the finite element solution $\hat{u}^{h_1}(x,\omega_s)$ from equation (41).
(4) Calculate the reference solution for the two-stage stochastic homogenization method as follows

$$\hat{u}^{L,h_1}(x) = \frac{1}{L}\sum_{s=1}^{L}\hat{u}^{h_1}(x,\omega_s).$$

5. Numerical examples

In this section, 2D numerical experiments based on different heterogeneous structures are conducted to verify the accuracy and efficiency of our method. Numerical experiments in Section 5.1 are performed on a desktop workstation with 32 GB of memory and a 2.1 GHz Xeon 5218R CPU, while those in Section 5.2 are conducted on a desktop workstation with 64 GB of memory and a 2.8 GHz Core i9 CPU. In the following two examples, we consider $f(x) = 15$, with the cell $\mathcal{Q}_M$ taken as $Q = (0,1)^2$ and $M = 1$, and the computational domain $D = (0,1)^2$ with $\varepsilon = 1/11$. We investigate the numerical empirical mean μ_L as defined in (36), which is used in the two-stage stochastic homogenization method.

Case 1: Heterogeneous materials with deterministic structures and random coefficients, as shown in Fig. 3(a). The (i,j)-th element of $A^\varepsilon(x,\omega)$ in the diffusion equation (1) is given by

(42)
$$a_{ij}(\frac{x}{\varepsilon},\omega) = \begin{cases} 5\delta_{ij} + (1.2+\sin(2\pi\frac{x^{(1)}}{\varepsilon})\sin(2\pi\frac{x^{(2)}}{\varepsilon})\delta_{ij})Z_{\mathbf{k}}(\omega) & x \in \varepsilon(Q_1+\mathbf{k}), \\ 550\delta_{ij} + (66+\sin(2\pi\frac{x^{(1)}}{\varepsilon})\sin(2\pi\frac{x^{(2)}}{\varepsilon})\delta_{ij})Z_{\mathbf{k}}(\omega) & x \in \varepsilon(Q_2+\mathbf{k}), \end{cases}$$

where $x = (x^{(1)}, x^{(2)})$, the inclusion $Q_2 = (0.2, 0.8)^2$, the matrix $Q_1 = (0,1) \setminus Q_2$, and the i.i.d. random variables $\left(Z_{\mathbf{k}}(\omega)\right)_{\mathbf{k}\in\mathbb{Z}^2}$ follow a truncated normal distribution. The probability density function for the truncated normal distribution is given by

$$\rho(\omega,-b,b) = \begin{cases} \dfrac{\psi(\omega)}{\zeta(b)-\zeta(-b)} & \omega \in [-b,b], \\ 0 & \text{otherwise}, \end{cases} \tag{43}$$

where $\psi(\omega) = \frac{1}{\sqrt{2\pi}}\exp\left(-\frac{1}{2}\omega^2\right)$, $\zeta(\omega) = \frac{1}{2}(1+\operatorname{erf}(\omega/\sqrt{2}))$, and $b = 1.5$.

Case 2: Heterogeneous materials with deterministic structures and random coefficients. Let $\mathcal{Q}_M = Q = Q_1 \cup Q_2$, where $Q_1 \cap Q_2 = \varnothing$, and Q_2 contains 5 elliptical inclusions, as shown in Fig. 3(b). The (i,j)-th element of $A^\varepsilon(x,\omega)$ in the diffusion equation (1) is given by the random coefficients in (42).

Case 3: Heterogeneous materials with random structures and deterministic coefficients. The computational domain D is decomposed into 11×11 elements, each containing 13 elliptical inclusions sampled with a uniformly random distribution parameter ω, as shown in Fig. 3(c). The (i,j)-th element of $A^\varepsilon(x,\omega)$ in the diffusion equation (1) is given by the random coefficients in (42).

$$a_{ij}(\frac{x}{\varepsilon},\omega) = \begin{cases} 5\delta_{ij} & x \in D_1(\omega), \\ 550\delta_{ij} & x \in D_2(\omega). \end{cases} \tag{44}$$

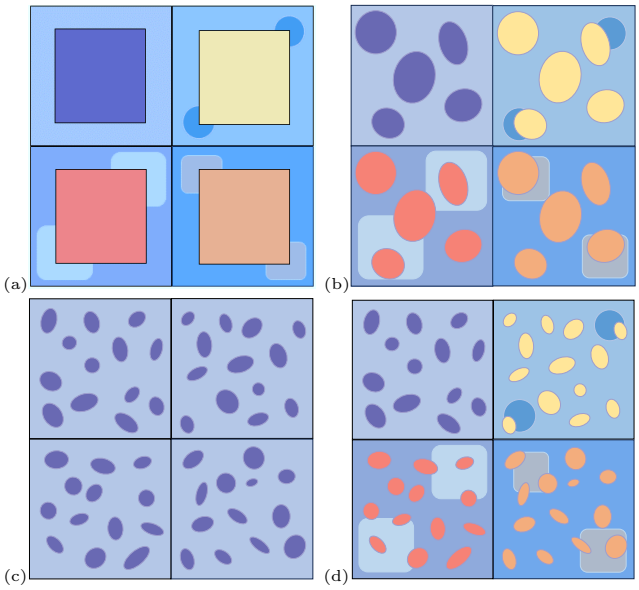

FIGURE 3. The setup of heterogeneous structures consists of four types of RVEs: (a) fixed inclusion structure with random coefficients; (b) fixed elliptical inclusion structure with random coefficients; (c) random elliptical inclusion structure with fixed coefficients; and (d) random elliptical inclusion structure with random coefficients.

Case 4: Heterogeneous materials with random structures and random coefficients. The computational domain D is decomposed into 11×11 elements, each containing 10 elliptical inclusions sampled with a uniform random distribution parameter ω_1, as shown in Fig. 3(d). $D_1(\omega_1)$ and $D_2(\omega_1)$ are defined as in Case 3. The (i, j)-th element of $A^\varepsilon(x, \omega)$ in the diffusion equation (1) is

$$a_{ij}(\frac{x}{\varepsilon}, \omega) = \begin{cases} 5\delta_{ij} + (1.2 + \sin(2\pi\frac{x^{(1)}}{\varepsilon})\sin(2\pi\frac{x^{(2)}}{\varepsilon})\delta_{ij})Z_{\mathbf{k}}(\omega_2) \\ \qquad x \in D_1(\omega_1) \cap \varepsilon(Q_1 + \mathbf{k}), \\ 550\delta_{ij} + (66 + \sin(2\pi\frac{x^{(1)}}{\varepsilon})\sin(2\pi\frac{x^{(2)}}{\varepsilon})\delta_{ij})Z_{\mathbf{k}}(\omega_2) \\ \qquad x \in D_2(\omega_1) \cap \varepsilon(Q_2 + \mathbf{k}), \end{cases} \tag{45}$$

where i.i.d. random variables $\big(Z_{\mathbf{k}}(\omega)\big)_{\mathbf{k}\in\mathbb{Z}^2}$ follow the truncated normal distribution defined in (43).

5.1. Verification of the RVE method. To verify the proposed method, the cut-off method defined in the literature [13, 14] was used to calculate $A_N^\star = (\hat{a}_{ij,N}^\star(\omega))$ as the reference solution. For Case 1 and Case 2, setting $L = N^2$ facilitated a comparison between μ_L and $A_N^\star$. For $N = 22$, 20 independent and identically distributed (i.i.d.) samples were generated, each containing 484 samples. Twenty independent repetitions were performed, and their means were taken as the final value of μ_L. Table 1 presents the numerical expectations, variances, and total computation times of the equivalent coefficient matrices for both methods in Case 1 and Case 2. The numerical results indicate that the equivalent coefficient matrix

μ_L provides a good approximation of the random homogenized matrix $A^\star$, and the proposed method is approximately eight times more efficient than the traditional stochastic homogenization method.

TABLE 1. Comparison of the numerical expectation and variance of the equivalent matrix obtained using our method and the traditional stochastic homogenization method [13, 14].

		Expectation	Variance	Computing time (s)
Case 1	$\mu^0_{11,L}$	11.474	0.146	39.8
	$\hat{a}^\star_{11,N}$	11.006	0.152	244.9
Case 2	$\mu^0_{11,L}$	9.912	0.122	454.1
	$\hat{a}^\star_{11,N}$	9.372	0.128	3081.9

5.2. Verification of the two-stage method. The the numerical empirical mean μ_L as defined in (36) for equivalent coefficient matrix $\hat{A}(x,\omega)$ was used to solve the random diffusion equation in (15), with the results serving as a reference solution. For $L = 1000$, the focus shifted to more complex cases: Case 3, which involves a randomly structured matrix with fixed coefficients, and Case 4, with both random structure and coefficients. This was analyzed by varying the number of iterations n in (39), employing a two-stage homogenization method. The relative L^2 norm error of the proposed method is defined as $\|\hat{u}_n^{0,h_0} - \hat{u}^{L,h_1}\|_{L^2(D)}/\|\hat{u}^{L,h_1}\|_{L^2(D)}$. The L^2 relative errors of the two-stage homogenized solutions compared to the reference solution are shown in Table 2, while Fig. 4 presents a visual line graph. It is observed that the L^2 relative error for Case 3 significantly decreases as n increases, and the L^2 relative error for Case 4 decreases with oscillations, reaching below 10e-6 at $n = 6$.

TABLE 2. The L^2 norm error of the two-stage homogenization solutions, obtained by iterating n times in (24), is compared to the reference solutions.

	n	0	1	2	3	4	5	6
error	Case 3	4.20e-3	2.71e-3	1.36e-4	6.79e-5	2.66e-6	1.92e-6	2.94e-7
	Case 4	2.49e-2	2.31e-2	8.45e-5	1.27e-3	4.71e-5	1.13e-4	9.23e-6

The Fig. 5, Fig. 6, Fig. 7, and Fig. 8 display the cloud maps of the two-stage stochastic homogenization solutions obtained from the EMC method after 6 iterations and the reference solutions for Cases 1, 2, 3, and 4, along with the cloud maps of their absolute errors. The maximum absolute error is found to be within the range of 10e-6 to 10e-8.

Table 3 presents the relative L^2 errors for Cases 1, 2, 3, and 4 compared to the reference solution, showing that the relative errors range from 10e-6 to 10e-7, demonstrating the consistency of the results, which can be regarded as equivalent. In particular, the proposed method only requires solving equations (22) and (23) with deterministic coefficients and random sources, which can be directly solved using an LU solver, significantly reducing computational costs.

The time comparison between the two-stage homogenization method and the reference method, shown in Table 4, indicates that the time cost of the proposed

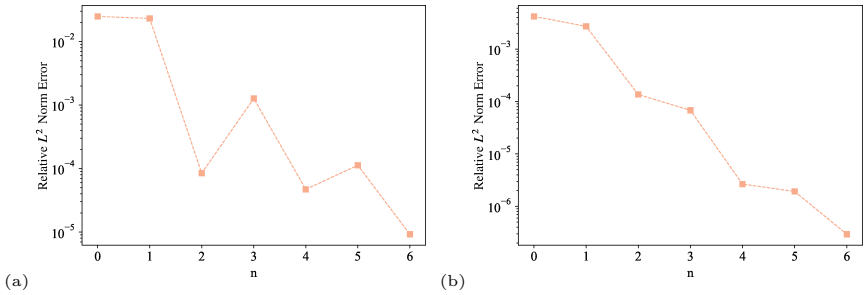

FIGURE 4. The relative L^2 norm error between the solutions obtained from the two-stage homogenization method and the reference solutions varies with the iteration count of the EMC algorithm: (a) Case 3, (b) Case 4.

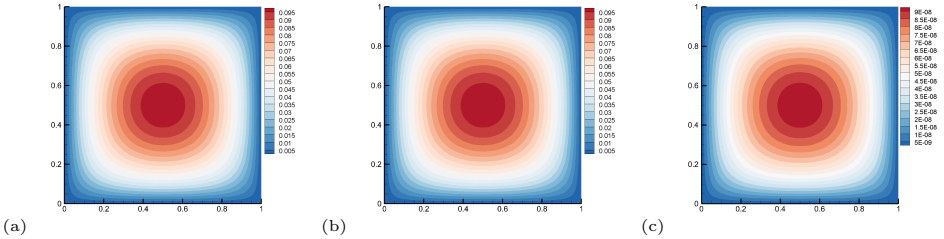

FIGURE 5. The contour plots of the solutions with a grid size of $h_0 = h_1 = 1/100$, are as follows: (a) The two-stage stochastic homogenization solution u_n^{0,h_0} for Case 1; (b) The reference solution $\hat{u}^{L,h_1}$ for Case 1; (c) The distribution of absolute errors between u^{n,h_0} and $\hat{u}^{L,h_1}$ of Case 1.

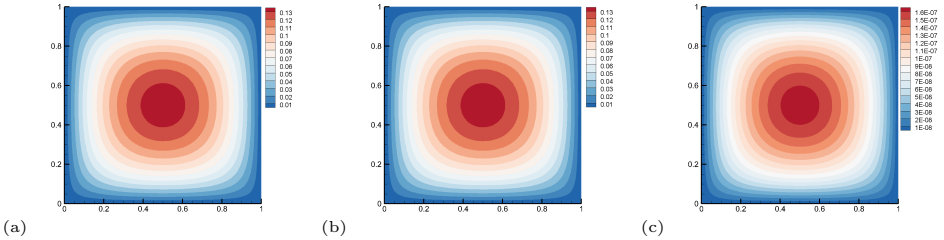

FIGURE 6. The contour plots of the solutions with a grid size of $h_0 = h_1 = 1/100$ are as follows: (a) The two-stage stochastic homogenization solution u_n^{0,h_0} for Case 2; (b) The reference solution $\hat{u}^{L,h_1}$ for Case 2; (c) The distribution of absolute errors between u^{n,h_0} and $\hat{u}^{L,h_1}$ of Case 2.

TABLE 3. The relative L^2 norm error between the two-stage homogenization solutions and the reference solutions.

	Case 1	Case 2	Case 3	Case 4
error	9.48e-7	1.22e-6	2.94e-7	9.23e-6

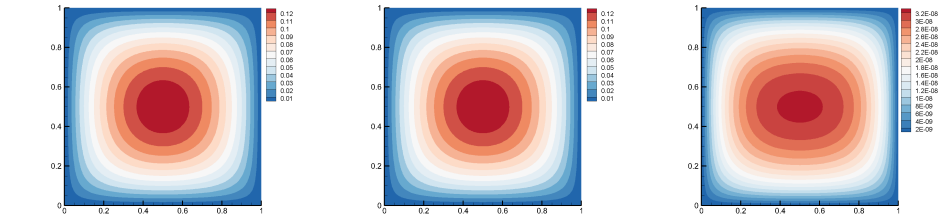

(a) (b) (c)

FIGURE 7. The contour plots of the solutions with a grid size of $h_0 = h_1 = 1/100$ are as follows: (a) The two-stage stochastic homogenization solution u_n^{0,h_0} for Case 3; (b) The reference solution $\hat{u}^{L,h_1}$ for Case 3; (c) The distribution of absolute errors between u^{n,h_0} and $\hat{u}^{L,h_1}$ of Case 3.

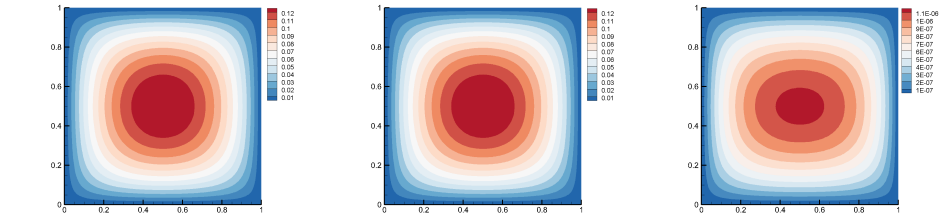

(a) (b) (c)

FIGURE 8. The contour plots of the solutions with a grid size of $h_0 = h_1 = 1/100$ are as follows: (a) The two-stage stochastic homogenization solution u_n^{0,h_0} for Case 4; (b) The reference solution $\hat{u}^{L,h_1}$ for Case 4; (c) The distribution of absolute errors between u^{n,h_0} and $\hat{u}^{L,h_1}$ of Case 4.

method is 4-5 times lower than that of the classical Monte Carlo method. This is because that the iterative equations (22) and (23) in our proposed method involve the same deterministic coefficients and a random source. Consequently, an LU direct solver can be employed to obtain numerical solutions efficiently, leading to significant computational cost savings. In summary, the two-stage stochastic homogenization method proposed in this paper is both accurate and efficient.

TABLE 4. Comparison of computational time between two-stage homogenization solutions and reference solutions.

		Case 1	Case 2	Case 3	Case 4
time(s)	RVE-EMC	75.924	107.47	83.216	87.824
	Reference	324.28	383.89	434.12	761.01

6. Conclusions

In this paper, we present a solution method for the diffusion equations of heterogeneous materials with random and rapidly oscillating coefficients. The main contribution of this work is the proposal of an efficient two-stage stochastic homogenization method, which combines the representative volume element approach with

an ensemble-based Monte Carlo algorithm. Our method separates the computational challenges arising from both the spatial rapid oscillation and the randomness of the solution, employing distinct strategies to address each of these difficulties. Numerical examples demonstrate the efficiency and effectiveness of the proposed method.

Acknowledgments

The work was supported by the Guangdong Basic and Applied Basic Research Foundation (2024A1515011597), National Natural Science Foundation of China (12301675), Natural Science Foundation of Shaanxi Province of China (2024JC-YBMS-012), National Key R&D Program of China with the grant (2020YFA-0713603) and the Degree and Graduate Education Research Fund of Northwestern Polytechnical University.

References

[1] R. M. German. Particulate composites. Springer, 2016.
[2] H. Herrmann and J. Schnell. Short fibre reinforced cementitious composites and ceramics. Springer, 2019.
[3] S. Sharma. Mechanics of particle-and fiber-reinforced polymer nanocomposites: from nanoscale to continuum simulations. John Wiley & Sons, 2021.
[4] M. Wang, J. Wang, N. Pan, and S. Chen. Mesoscopic predictions of the effective thermal conductivity for microscale random porous media. Physical Review E, 75: 036702, 2007.
[5] G. Stefanou, D. Savvas, and M. Papadrakakis. Stochastic finite element analysis of composite structures based on mesoscale random fields of material properties. Computer Methods in Applied Mechanics and Engineering, 326: 319–337, 2017.
[6] Z. Li, Q. Ma, and J. Cui. Multi-scale modal analysis for axisymmetric and spherical symmetric structures with periodic configurations. Computer Methods in Applied Mechanics and Engineering, 317: 1068–1101, 2017.
[7] Z. Yang, X. Guan, J. Cui, H. Dong, Y. Wu, and J. Zhang. Stochastic multiscale heat transfer analysis of heterogeneous materials with multiple random configurations. Communications in Computational Physics, 27(2): 431–459, 2020.
[8] O. S. Yakovenko, L. Y. Matzui, L. L. Vovchenko, V. V. Oliynyk, V. V. Zagorodnii, S. V. Trukhanov, and A. V. Trukhanov. Electromagnetic properties of carbon nanotube/$BaFe_{12-x}Ga_xO_{19}$/Epoxy composites with random and oriented filler distributions. Nanomaterials, 11(11): 2873, 2021.
[9] Z. Yang, X. Wu, X. He, and X. Guan. A multiscale analysis-assisted two-stage reduced-order deep learning approach for effective thermal conductivity of arbitrary contrast heterogeneous materials. Engineering Applications of Artificial Intelligence, 136: 108916, 2024.
[10] A. Anantharaman, R. Costaouec, C. L. Bris, F. Legoll, and F. Thomines. Introduction to numerical stochastic homogenization and the related computational challenges: Some recent developments. In multiscale modeling and analysis for materials simulation, 197–272. World Scientific, 2012.
[11] J. C. Mourrat. An informal introduction to quantitative stochastic homogenization. Journal of Mathematical Physics, 60(3): 031506, 2019.
[12] M. Duerinckx, A. Gloria, and F. Otto. The structure of fluctuations in stochastic homogenization. Communications in Mathematical Physics, 377(1): 259–306, 2020.
[13] A. Gloria. Numerical approximation of effective coefficients in stochastic homogenization of discrete elliptic equations. ESAIM: Mathematical Modelling and Numerical Analysis, 46(1): 1–38, 2012.
[14] S. Armstrong, T. Kuusi, and J. C. Mourrat. Quantitative stochastic homogenization and large-scale regularity, volume 352. Springer, 2019.
[15] Z. Yang, J. Cui, and Y. Wu. Second-order two-scale analysis method for dynamic thermomechanical problems in periodic structure. International Journal of Numerical Analysis and Modeling, 12: 144–161, 2015.

[16] M. Schneider, M. Josien, and F. Otto. Representative volume elements for matrix-inclusion composites-a computational study on the effects of an improper treatment of particles intersecting the boundary and the benefits of periodizing the ensemble. Journal of the Mechanics and Physics of Solids, 158: 104652, 2022.
[17] O. Vallmaj, A. Arteiro, and J.M. Guerrero. Micromechanical analysis of composite materials considering material variability and microvoids. International Journal of Mechanical Sciences, 263: 108781, 2024.
[18] F. Aldakheel, E. Elsayed, and T. Zohdi. Efficient multiscale modeling of heterogeneous materials using deep neural networks. Computational Mechanics, 72(1): 155-171, 2023.
[19] X. Guan, X. Liu, X. Jia, Y. Yuan, J. Cui, and H. A. Mang. A stochastic multiscale model for predicting mechanical properties of fiber reinforced concrete. International Journal of Solids and Structures, 56-57: 280–289, 2015.
[20] M. A. Tashkinov. Multipoint stochastic approach to localization of microscale elastic behavior of random heterogeneous media. Computers & Structures, 249: 106474, 2021.
[21] Z. Yang, Y. Zhang, H. Dong, J. Cui, X. Guan, and Z. Yang. High-order three-scale method for mechanical behavior analysis of composite structures with multiple periodic configurations. Composites Science and Technology, 152: 198–210, 2017.
[22] A. B. Owen and P. W. Glynn. Monte Carlo and quasi-Monte Carlo methods. Springer, 2016.
[23] K. Liu and B. M. Rivire. Discontinuous Galerkin methods for elliptic partial differential equations with random coefficients. International Journal of Computer Mathematics, 90(11): 2477–2490, 2013.
[24] I. Babuska, R. Tempone, and G. E. Zouraris. Galerkin finite element approximations of stochastic elliptic partial differential equations. SIAM Journal on Numerical Analysis, 42(2): 800–825, 2004.
[25] Z. Fang, J. Li, T. Tang, and T. Zhou. Efficient stochastic Galerkin methods for Maxwells equations with random inputs. Journal of Scientific Computing, 80: 248–267, 2019.
[26] M. D. Gunzburger, C. G. Webster, and G. Zhang. Stochastic finite element methods for partial differential equations with random input data. Acta Numerica, 23: 521C650, 2014.
[27] J. Beck, R. Tempone, F. Nobile, and L. Tamellini. On the optimal polynomial approximation of stochastic pdes by Galerkin and collocation methods. Mathematical Models and Methods in Applied Sciences, 22(09): 1250023, 2012.
[28] M. Gunzburger, N. Jiang, and Z. Wang. An efficient algorithm for simulating ensembles of parameterized flow problems. IMA Journal of Numerical Analysis, 39(3): 1180–1205, 2019.
[29] Y. Luo and Z. Wang. An ensemble algorithm for numerical solutions to deterministic and random parabolic pdes. SIAM Journal on Numerical Analysis, 56(2): 859–876, 2018.
[30] X. Feng, Y. Luo, L. Vo, and Z. Wang. An efficient iterative method for solving parameter-dependent and random convection–diffusion problems. Journal of Scientific Computing, 90(2): 1–26, 2022.
[31] J. Yong, C. Ye, X. Luo, and S. Sun. Improved error estimates of ensemble Monte Carlo methods for random transient heat equations with uncertain inputs. Computational and Applied Mathematics, 44(1): 58, 2025.
[32] X. Feng, J. Lin, and C. Lorton. An efficient Monte Carlo interior penalty discontinuous Galerkin method for the time-harmonic Maxwells Equations with random coefficients. Journal of Scientific Computing, 80: 1498C1528, 2019.
[33] S. Zhang, Z. Yang, and X. Guan. Multi-modes multiscale approach of heat transfer problems in heterogeneous solids with uncertain thermal conductivity. Advances in Applied Mathematics and Mechanics, 15(1): 69-93, 2023.
[34] X. Feng, J. Lin, and P. Nicholls. An efficient Monte Carlo-transformed field expansion method for electromagnetic wave scattering by random rough surfaces. Communications in Computational Physics, 23: 685–705, 2018.
[35] Z. Yang, J. Huang, X. Feng, and X. Guan. An efficient multimodes monte carlo homogenization method for random materials. SIAM Journal on Scientific Computing, 44(3): A1752–A1774, 2022.
[36] X. Feng, J. Lin, and C. Lorton. A multimodes monte carlo finite element method for elliptic partial differential equations with random coefficients. International Journal for Uncertainty Quantification, 6(5): 429–443, 2016.
[37] D. Cioranescu and P. Donato. An introduction to homogenization, volume 17. Oxford University Press, 1999.

Shenzhen Research Institute of Northwestern Polytechnical University, Shenzhen 518063, China

School of Mathematics and Statistics, Northwestern Polytechnical University, Xian 710072, PR China

Zhuhai Simark technology Co., Ltd., Zhuhai 519000, PR China

School of Mathematics, Northwest University, Xian 710027, PR China

School of Mathematics and Statistics, Northwestern Polytechnical University, Xian 710072, PR China
E-mail: zhaojf@nwpu.edu.cn